J Therm Anal Calorim (2011) 103:897–902
DOI 10.1007/s10973-010-1087-z

Importance of the interlayer orientation in borate-intercalating layered double hydroxides

A study on thermal decomposition kinetics and mechanism

Ahmet Nedim Ay

Received: 6 September 2010 / Accepted: 30 September 2010 / Published online: 17 October 2010

Abstract Thermal decomposition kinetics and mechanism of layered double hydroxides (LDHs) intercalating different amounts and types of borate ions were studied using Coats–Redfern integral and Achar differential methods. The results revealed that the Coats–Redfern integral method is more appropriate than the Achar differential method for evaluation of the nonisothermal thermogravimetric decomposition data. The first-order Avrami-Erofe'ev A_1 mechanism was found to be the best fitting kinetic model for almost all samples. In addition to the amount and type of the intercalated borate ion, interlayer orientation was also of importance in determining the chemical and thermal stabilities and hence the decomposition kinetics of the studied compounds.

Keywords Layered double hydroxides · Borate · Intercalation · Decomposition kinetics · Orientation

Introduction

Layered double hydroxides consist of positively charged metal hydroxide layers and exchangeable interlayer ions and water molecules. The general formula of these lamellar solids is $[M^{II}_{1-x}M^{III}_{x}(OH)_2]^{x+}[A^{n-}_{x/n}\cdot yH_2O]^{x-}$ where M^{II} and M^{III} are divalent and trivalent metal cations, respectively, A^{n-} is a charge balancing n-valent anion. The chemical and physical properties of these compounds strongly depend not only on the type of the metal or interlayer ions but also on the synthesis conditions and M^{II}/M^{III} molar ratios [1]. Therefore, these materials are best fitted to the term "tailored materials." Every LDH hides a secret in its nanogalleries. In recent years, countless researches have been proceeding to expose this secret in catalytic, ion exchange, magnetic, and medical processes.

Boron compounds have been used as high performance materials with chemical and temperature resistance, conductivity, and hardness properties [2, 3] as catalysts in many chemical reactions [1] and in medicine as boron neutron capture therapy (BNCT) agents [4]. LDHs, containing boron compounds possess very interesting properties and may find unexpected uses in many areas. They show better thermal stabilities than nitrate- or carbonate-LDHs [5, 6] and can be used as effective catalysts in acid-catalysed reactions such as Beckmann rearrangement of cyclohexanone oxime to caprolactam and aldol condensation reactions [5, 7, 8].

Many scientists have been studying the intercalation of boron compounds into the LDH galleries since the first borate incorporation was reported by Chen and Lin [9] in 1992. Preparation of triborate pillared LDH by direct synthesis was then reported by Bhattacharyya and Hall [10]. Li et al. [11], Parker et al. [12], Del Arco et al. [13], and Shi et al. [14] synthesized and investigated borate-LDH samples prepared by ion exchange. A very simple preparation, direct synthesis by mortar-grinding method was reported by our laboratory in 2009 [15].

Thermal decomposition kinetics and mechanism is important for the design and optimization of materials [16]. Studying the thermal decomposition kinetics and mechanism of borate intercalated LDHs can therefore provide valuable information about the preparation of boron containing mixed oxide catalysts and their properties. Kinetic analysis of these compounds by nonisothermal methods appears to be more advantageous as the sudden evaporation

A. N. Ay (✉)
Chemistry Department, Hacettepe University, Beytepe Campus, 06800 Ankara, Turkey
e-mail: ay@hacettepe.edu.tr

of water molecules from the interlayer galleries may cause unexpected decomposition routes in isothermal heating processes. We recently investigated the chemical and structural characterization of borate-LDHs prepared by co-precipitation and ion-exchange methods [17]. Here we report the thermal decomposition mechanism and kinetics of borate-LDHs by employing Coats–Redfern integral and Achar differential methods [18–20].

The Coats–Redfern integral method can be applied to solid state decomposition reactions assuming the reaction orders 0, 1/2, 2/3, 3/4, and 1 [19, 20]. This method is less affected from the experimental factors such as sample size, heating rate and can be applied to nonisothermal thermogravimetric data [20]. The order is assessed according to the linearity of the applied kinetic model plot line. The Coats–Redfern equation is:

$$\log\left[\frac{f(\alpha)}{T^2}\right] = \log\left[\frac{AR}{\beta E_a}\left(1-\frac{2RT}{E_a}\right)\right] - \frac{E_a}{2.3RT} \quad (1)$$

and the reaction 1 leads to reaction 2 if the $(2RT/E) << 1$,

$$\log\left[\frac{f(\alpha)}{T^2}\right] = \log\left[\frac{AR}{\beta E_a}\right] - \frac{E_a}{2.3RT} \quad (2)$$

$f(\alpha)$ is the decomposition fraction (α) function depends on the integral mechanism, E_a is the activation energy which is calculated from the slope of the line ($-E_a/2.3R$) obtained by plotting $\log[f(\alpha)/T^2]$ versus $1/T$. A and β are pre-exponential factor and constant heating rate, respectively.

The Achar differential method can be applied to all reaction mechanisms if the reaction rate can be given as a function of α [19, 20]. The equation is:

$$\log\left[\frac{\mathrm{d}(\alpha)/\mathrm{d}T}{g(\alpha)}\right] = \log\frac{A}{\beta} - \frac{E_a}{2.3RT} \quad (3)$$

Activation energy and the pre-exponential constant can be calculated from the plot of $[(\mathrm{d}(\alpha)/\mathrm{d}(T)/g(\alpha)]$ versus $1/T$.

The commonly used $f(\alpha)$ and $g(\alpha)$ functions are listed in Table 1 [16, 20, 21].

Materials and methods

The synthesis and the characterization of the products have been described previously [6, 17]. The precursor nitrate-LDH (N-LDH) was synthesized by co-precipitation method and borate intercalated LDHs were prepared by exchanging the interlayer nitrate ions with boric acid solution (i) without making any pH adjustment (B-LDH), (ii) at pH 9 (B-LDH-9), and (iii) 12 (B-LDH-12) by adjusting with NaOH solution.

Thermal analyses (TG, DTA) were performed by a Shimadzu DTG-60H system, in dynamic nitrogen atmosphere (50 mL/min) at heating rates of 5, 10, and 15 °C/min in the temperature range from 25 to 900 °C. E_a and A were determined from the best fit line of data points plotted according to the kinetic model with the highest linear correlation coefficient ($r > 0.99$).

Results and discussion

The borate intercalated LDHs were obtained by exchanging the interlayer nitrate ions with boric acid solution at different pH values. The products have been shown to contain different types of borate species in the interlayer galleries depending on the reaction pH, although the principal borate source was boric acid (Table 2) [17]. It is known that in aqueous solutions, the distribution of borate species is affected by the pH, concentration, and temperature of the solution [22, 23]. For LDHs, the nature of the interlayer region depends also on the local pH variations at the inner surfaces of the galleries [6, 17, 24].

Thermal decomposition curves of the products recorded at three different heating rates (5, 10, 15 °C/min) are shown in Fig. 1. The products displayed a similar thermal behavior regardless of the heating rate, so the kinetic analyses were therefore performed with the data obtained at 10 °C/min. The first derivative curves (DTG) of the thermograms recorded at 10 °C/min are seen in Fig. 2. The

Table 1 Commonly used algebraic expressions for $f(\alpha)$ and $g(\alpha)$

Kinetic model	Symbol	$f(\alpha)$	$g(\alpha)$
Reaction order/$n = 1$	N_1	$-\log(1-\alpha)$	$(1-\alpha)^n$
Reaction order/$n < 1$	N_0, $N_{1/2}$, $N_{2/3}$, $N_{3/4}$	$[1-(1-\alpha)^{1-n}/(1-n)]$	$(1-\alpha)^n/(1-n)$; $n < 1$
One-dimensional diffusion	D_1	α^2	$1/2\alpha$
Two-dimensional diffusion	D_2	$(1-\alpha)\ln(1-\alpha) + \alpha$	$[-\ln(1-\alpha)]^{-1}$
Three-dimensional diffusion	D_3	$[1-(1-\alpha)^{1/3}]^2$	$1.5(1-\alpha)^{2/3}[1-(1-\alpha)^{1/3}]^{-1}$
Nucleation and nuclei growth/Avrami-Erofe'ev;1	A_1	$-\ln(1-\alpha)$	$1-\alpha$
Nucleation and nuclei growth/Avrami-Erofe'ev;1.5	$A_{1.5}$	$[-\ln(1-\alpha)]^{2/3}$	$1.5(1-\alpha)[-\ln(1-\alpha)]^{1/3}$
Nucleation and nuclei growth/Avrami-Erofe'ev;2	A_2	$[-\ln(1-\alpha)]^{1/2}$	$2(1-\alpha)[-\ln(1-\alpha)]^{1/2}$
Nucleation and nuclei growth/Avrami-Erofe'ev;3	A_3	$[-\ln(1-\alpha)]^{1/3}$	$3(1-\alpha)[-\ln(1-\alpha)]^{2/3}$

Table 2 Chemical compositions of borate-LDH samples

Sample	B/%	Formula
N-LDH	–	$[Mg_{0.58}Al_{0.42}(OH)_2](NO_3)_{0.42}{\cdot}0.6H_2O$
B-LDH	3.4	$[Mg_{0.49}Al_{0.51}(OH)_2][B_3O_3(OH)_4]_{0.11}\ (NO_3)_{0.16}\ (CO_3)_{0.12}{\cdot}0.5H_2O$
B-LDH-9	3.8	$[Mg_{0.57}Al_{0.43}(OH)_2][B_4O_5(OH)_4]_{0.084}\ (NO_3)_{0.0085}\ (CO_3)_{0.125}{\cdot}0.5H_2O$
B-LDH-12	1.2	$[Mg_{0.68}Al_{0.32}(OH)_2][B_3O_3(OH)_4]_{0.037}(NO_3)_{0.063}\ (CO_3)_{0.11}{\cdot}0.6H_2O$

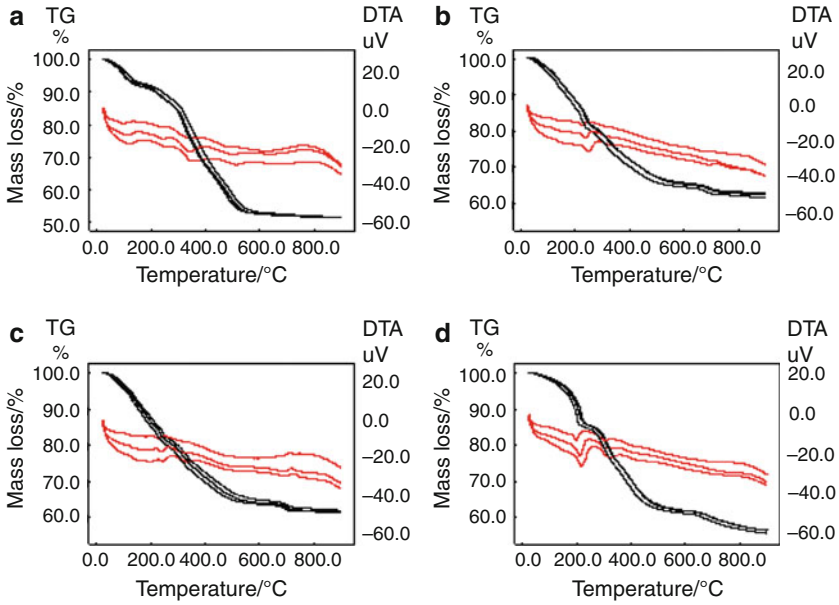

Fig. 1 Thermal decomposition of the products; **a** N-LDH, **b** B-LDH, **c** B-LDH-9, **d** B-LDH-12 (TG and DTA curves)

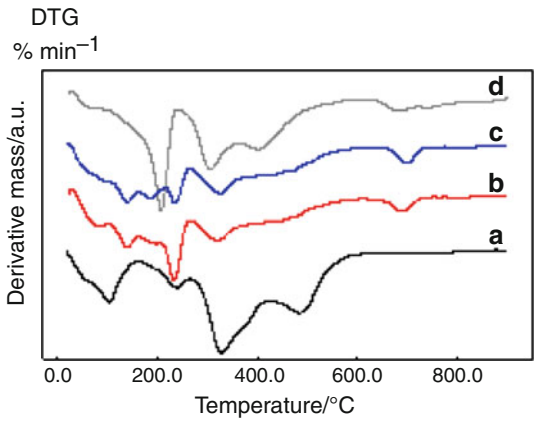

Fig. 2 DTG curves of the products; *a* N-LDH, *b* B-LDH, *c* B-LDH-9, *d* B-LDH-12

results obtained for different B-LDH samples were correlated with each other and also with those for N-LDH.

Decomposition of N-LDH proceeds in this order: surface water evaporates below 140 °C, removal of interlayer water molecules then starts and continues up to 375 °C. Dehydroxylation, removal of the hydroxyl groups from the layers as water vapour, and decomposition of the interlayer anions occur at higher temperatures up to 600 °C [6]

Table 3 Thermal decomposition stages of the products

Products	Stages/°C				
	1	2	3	4	5
N-LDH	80–140	210–260	290–400	450–550	
B-LDH	100-160	210–255	270–360	370–550	600–740
B-LDH-9	100–160	210–255	270–360	370–550	645–740
B-LDH-12	100–235	260–330	370–550	635–720	

B-LDH and B-LDH-9 showed similar decomposition curves since they have similar boron contents with respect to B-LDH-12. The endothermic DTA peaks around 85 and 138 °C correspond to the loss of surface and interlayer water. The peaks between 180 and 550 °C correspond to dehydroxylation of the LDH sheets and of the interlayer anions, $[B_4O_5(OH)_4]^{2-}$ and $[B_3O_3(OH)_4]^{-}$. The exothermic DTA peaks at 715 and 717 °C can be assigned to the complete lattice collapse and phase transition to a mixed oxide system [9, 11]. For B-LDH-12, although the TG curve was similar, the DTG peak temperatures shifted approximately 20 °C to the lower temperatures. Figure 2 verifies the effect of the boron content on thermal stability. B-LDH-9 has the highest boron content (Table 2) and

Table 4 Calculated correlation coefficients (r^2) for the used kinetic models

	Kinetic models[a]											
	A_1		$A_{1.5}$		A_2		A_3		D_1		D_2	
Stages	I	II	I	II	I	II	I	II	I	II	I	II
N-LDH												
1	**0.9919**	0.9467	0.9907	0.8060	0.9893	0.5682	0.9854	0.0472	0.9069	0.8898	0.9501	0.8276
2	0.9937	0.9537	0.9933	0.9013	0.9929	0.6813	0.9919	0.2376	0.9379	0.8344	0.9689	0.9633
3	**0.9909**	0.9321	0.9896	0.5062	0.988	0.6761	0.9839	0.3150	0.9317	0.7986	0.9581	0.9199
4	**0.9955**	0.9382	0.9951	0.8742	0.9946	0.7020	0.9935	0.3707	0.9284	0.5980	0.9226	0.9222
B-LDH												
1	**0.9984**	0.9691	0.9982	0.6708	0.9981	0.8334	0.9976	0.1405	0.9616	0.8903	0.9827	0.9677
2	**0.9907**	0.9847	0.9903	0.6952	0.9898	0.7743	0.9889	0.0889	0.9062	0.5409	0.9536	0.8082
3	**0.9944**	0.9302	0.9938	0.8912	0.9931	0.6656	0.9914	0.3194	0.9204	0.8242	0.9670	0.9602
4	**0.9952**	0.9030	0.9935	0.9506	0.9931	0.5220	0.9864	0.2297	0.8001	0.3812	0.9437	0.8380
5	**0.9955**	0.9299	0.9952	0.2572	0.9949	0.6643	0.9946	0.3457	0.9525	0.6380	0.9826	0.8466
B-LDH-9												
1	**0.9983**	0.9715	0.9982	0.6993	0.9979	0.8212	0.9974	0.5018	0.9577	0.5364	0.9820	0.9648
2	**0.9901**	0.9776	0.9896	0.7560	0.9891	0.6838	0.9880	0.0023	0.9101	0.5871	0.9536	0.8403
3	**0.9940**	0.9288	0.9934	0.8620	0.9927	0.9328	0.9909	0.2993	0.9396	0.8364	0.9675	0.9641
4	**0.9927**	0.8445	0.9913	0.8645	0.9895	0.5426	0.9836	0.2971	0.9009	0.0011	0.9450	0.6837
5	**0.9912**	0.9030	0.9907	0.4209	0.9903	0.5791	0.9894	0.3378	0.9140	0.0581	0.9660	0.4442
B-LDH-12												
1	0.9676	0.8977	0.9633	0.6809	0.958	0.7273	0.9426	0.5342	0.9845	0.7968	**0.9920**	0.9332
2	**0.9930**	0.9758	0.9925	0.3159	0.9918	0.4004	0.9904	0.4100	0.9328	0.8917	0.9676	0.9371
3	**0.9926**	0.8460	0.9903	0.956	0.9892	0.4463	0.9834	0.1477	0.7347	0.2965	0.9364	0.3530
4	**0.9922**	0.9351	0.9918	0.8416	0.9914	0.6676	0.9905	0.308	0.9339	0.8108	0.9622	0.9438

	Kinetic models[a]											
	D_3		$n = 0$		$n = 1/2$		$n = 2/3$		$n = 3/4$		$n = 1$	
Stages	I	II	I	II	I	II	I	II	I	II	I	II
N-LDH												
1	0.9634	0.9699	0.8883	0.3700	0.9622	0.6709	0.9788	0.8737	0.9814	0.9112	0.9919	0.9467
2	0.9757	**0.9955**	0.9319	0.1360	0.9830	0.9763	0.9864	0.9719	0.9792	0.9672	0.9937	0.9537
3	0.9794	0.9758	0.9177	0.1466	0.9683	0.8901	0.9794	0.9253	0.9813	0.9315	0.9909	0.9321
4	0.9871	0.9938	0.9186	0.4542	0.9774	0.9716	0.9864	0.9671	0.9843	0.9591	0.9955	0.9382
B-LDH												
1	0.9625	0.9950	0.9268	0.4303	0.9912	0.9840	0.9809	0.9758	0.9790	0.9701	0.9984	0.9691
2	0.979	0.9555	0.8955	0.0208	0.9595	0.7242	0.9790	0.8639	0.9857	0.9213	0.9907	0.9847
3	0.9844	0.9902	0.9299	0.0274	0.9794	0.9507	0.9844	0.9467	0.9797	0.9425	0.9944	0.9302
4	0.9812	0.9657	0.8651	0.8728	0.9654	0.5534	0.9823	0.8627	0.9880	0.7956	0.9952	0.9030
5	0.9919	0.9638	0.9457	0.0146	0.9814	0.6916	0.9903	0.8327	0.9928	0.8737	0.9955	0.9299
B-LDH-9												
1	0.9912	0.9972	0.9490	0.0481	0.9907	0.9679	0.9912	0.9819	0.9831	0.9814	0.9983	0.9559
2	0.9810	0.9639	0.9002	0.1681	0.9638	0.7065	0.9810	0.8939	0.9852	0.9346	0.9901	0.9776
3	0.9847	0.9924	0.9309	0.0231	0.9797	0.9507	0.9847	0.9468	0.9801	0.9423	0.9940	0.9288
4	0.9608	0.8900	0.8604	0.7054	0.9682	0.5675	0.9833	0.7907	0.9826	0.8191	0.9927	0.8445
5	0.9872	0.8847	0.9232	0.1611	0.9737	0.2459	0.9872	0.5607	0.9908	0.6819	0.9912	0.9330
B-LDH-12												
1	0.9861	0.9767	0.9790	0.9218	0.9916	0.8826	0.9861	0.9085	0.9789	0.9138	0.9676	0.8977
2	0.9852	0.9832	0.9356	0.3793	0.9761	0.9283	0.9852	0.9628	0.9862	0.9706	0.9930	0.9758
3	0.9762	0.6494	0.8482	0.8741	0.9553	0.4606	0.9743	0.7516	0.9760	0.3366	0.9926	0.8460
4	0.9825	0.9850	0.9288	0.0167	0.9767	0.9181	0.9831	0.9359	0.9797	0.9377	0.9922	0.9351

[a] **I:** Coats–Redfern and **II:** Achar methods

displayed the highest DTG peak temperature (699 °C) corresponding to the lattice collapse while B-LDH-12 with the lowest boron content displayed the lowest DTG peak temperature (676 °C).

A careful examination of the DTG curves of the products revealed a multi-step decomposition behavior. Kinetic analyses were therefore performed by dividing the decomposition temperature range into stages (Table 3). The first two stages correspond to the removal of physically adsorbed water and free water molecules in the interlayer space. Dehydroxylation of the brucite layers takes place in the third stage and degradation of the intercalated ions proceed in the forth stage [17, 25, 26].

For N-LDH, the forth stage ends with the conversion to the spinel oxide phase while for B-LDH and B-LDH-12 there is an additional fifth stage corresponding to the collapse of the LDH structure, which reflects the effect of boron incorporation on the stabilization of LDHs. It has been reported that LDHs with different interlayer compositions undergo different decomposition pathways [27].

The correlation coefficients obtained by applying the Coats–Redfern and Achar methods to the stages given in Table 3 are summarized in Table 4 where the highest values are highlighted in bold. The higher r^2 values indicate that the Coats–Redfern method is more suitable than the Achar method for the determination of the kinetic model. With the Coats–Redfern method, first order Avrami-Erofoe'ev; A_1 mechanism was generally found to be the best fitting thermal decomposition kinetic model. A different model, 3D diffusion, fitted to the second decomposition stage of the N-LDH (dehydroxylation) while the first decomposition stage of B-LDH-12 appeared to be a 2D diffusion process.

The activation energy values listed in Table 5 verify the importance of the type and orientation of the interlayer borate anions on the decomposition of the products. B-LDH and B-LDH-9 samples have similar boron contents but different types of interlayer borate ions (Table 2). E_a values of B-LDH and B-LDH-9 were close to each other for the first four stages but different for the fifth stage. B-LDH-9 contains highly charged tetraborate ions, $[B_4O_5(OH)_4]^{2-}$, which help integration of the layers through stronger electrostatic interactions. More energy is needed for the complete lattice collapse and phase transition to a mixed oxide system for B-LDH-9 than for B-LDH which intercalates triborate ions, $[B_3O_3(OH)_4]^{-1}$. On the other hand, the surprisingly higher E_a value (357.13 kJ/mol) for B-LDH-12 could be rationalized by considering the orientation of the triborate ions between the layers. Powder X-ray diffraction (PXRD) analysis of the products indicated that the basal spaces (d_{003}) of B-LDH and B-LDH-12 are 9.58 and 7.69 Å, respectively [6]. The triborate anions should be located between the layers almost

Table 5 Kinetic parameters calculated according to the best fitting kinetic model

Sample	Stage 1			Stage 2			Stage 3			Stage 4			Stage 5		
	Eqn.[a]	E_a[b]	A	Eqn.[a]	E_a[b]	A	Eqn.[a]	E_a[b]	A	Eqn.[a]	E_a[b]	A	Eqn.[a]	E_a[b]	A
N-LDH	A_1	56.76	2.73×10^7	D_3	219.66	2.54×10^{20}	A_1	92.67	1.55×10^7	A_1	171.5	1.93×10^{11}			
B-LDH	A_1	82.16	1.45×10^{10}	A_1	209.01	2.57×10^{21}	A_1	111.84	2.06×10^9	A_1	68.11	1.08×10^4	A_1	262.09	5.37×10^{13}
B-LDH-9	A_1	79.05	5.43×10^9	A_1	195.16	7.19×10^{19}	A_1	114.26	3.01×10^9	A_1	75.22	3.78×10^4	A_1	357.49	7.05×10^{18}
B-LDH-12	D_2	87.69	5.79×10^8	A_1	145.76	4.92×10^{12}	A_1	78.57	1.48×10^5	A_1	357.13	1.03×10^{19}			

[a] Equation

[b] kJ mol^{-1}

laterally in B-LDH-12 [10]. The type of the intercalated borate anions between the galleries of the LDH has been deduced previously by PXRD, 2D ^{11}B MQMAS and ^{11}B MAS NMR spectra and Fourier transform infrared spectroscopy [17]. B-LDH and B-LDH-9 samples were shown to intercalate triborate and tetraborate anions, respectively. B-LDH-12 was surprisingly shown to contain triborate species although monoborate anions are expected to be the dominant borate species in the studied pH range according to Simon and Smith [23]. A plausible explanation could be that $B(OH)_4^-$ ions in the highly alkaline solution enter into the galleries where they convert to laterally oriented triborate species due to the local pH variations in the interlayer region [24].

As the electrostatic force is inversely proportional to the second power of distance, the laterally oriented triborate ions, though with lower charge densities, thus stabilize the LDH structure via strong electrostatic forces like B-LDH-9.

Conclusions

The results of this study have showed that the kinetics and mechanism of the thermal decomposition of borate intercalating LDHs depend on the type and the amount of the intercalated borate ions. The orientation of the interlayer anions is also important in stabilizing the lamellar structure by electrostatic interactions.

The decomposition mechanism of borate-LDHs is best described with Avrami-Erofoe'ev; A_1 nucleation and nuclei growth model while the first decomposition stage is diffusion controlled and fits the two-dimensional diffusion; D_2. Also the second decomposition stage of the N-LDH is diffusion controlled and fits the three-dimensional diffusion; D_3.

References

1. Vaccari A. Clays and catalysis: a promising future. Appl Clay Sci. 1999;14:161–98.
2. Lee JD. Concise inorganic chemistry. 4th ed. London: Chapman & Hall; 1991. pp. 359–98.
3. Coughlin JR. Inorganic borates: chemistry, human exposure, and health and regulatory guidelines. J Trace Elem Exp Med. 1996; 9:137–51.
4. Barth RF, Coderre JA, Vicente MGH, Blue TE. Boron neutron capture therapy of cancer: current status and future prospects. Clin Cancer Res. 2005;11:3987–4002.
5. Bechara R, D'Huysser A, Fournier M, Forni L, Fornasari G, Trifiro F, Vaccari A. Synthesis and characterization of boron hydrotalcite-like compounds as catalyst for gas-phase transposition of cyclohexanone-oxime. Catal Lett. 2002;82:59–67.
6. Ay AN. Synthesis and characterization of Mg-Al-layered double hydroxides intercalated by borate anions. PhD Thesis. Ankara; 2007.
7. Lin JT, Tsai SJ, Cheng S. Beckmann rearrangement of cyclohexanone oxime over borate-pillared LDHs. J Chin Chem Soc-Taip. 1999;46:779–83.
8. Dahlhoff G, Niederer JPM, Hölderich WF. ε-Caprolactam: new by-product free synthesis routes. Catal Rev. 2001;43:381–441.
9. Cheng S, Lin JT. Preparation and characterization of borate pillared anionic clays In: Ocelli ML, Robson HE, editors. Expanded clays and microporous solids. New York: van Nostrand Reinhold; 1992. pp. 170–86.
10. Bhattacharyya A, Hall BD. New triborate-pillared hydrotalcites. Inorg Chem. 1992;31:3869–70.
11. Li L, Ma S, Liu X, Yue Y, Hui J, Xu R, Bao Y, Rocha J. Synthesis and characterization of tetraborate pillared hydrotalcite. Chem Mater. 1996;8:204–8.
12. Parker LM, Milestone NB, Newman RH. The use of hydrotalcite as an anion absorbent. Ind Eng Chem Res. 1995;34:1196–202.
13. Del Arco M, Gutierrez S, Martin C, Rives V, Rocha J. Effect of the Mg:Al ratio on borate (or slicate)/nitrate exchange in hydrotalcite. J Solid State Chem. 2000;151:272–80.
14. Shi L, Li D, Wang J, Li S, Evans DG, Duan X. Synthesis and smoke-suppressant properties of a borate-intercalated layered double hydroxide. Clays Clay Miner. 2005;53:294–300.
15. Ay AN, Zümreoglu-Karan B, Mafra L. A simple mechanochemical route to layered double hydroxides: synthesis of hydrotalcite-like Mg-Al-NO_3-LDH by manual grinding in a mortar. Z Anorg Allg Chem. 2009;635:1470–5.
16. Wang L, Lü Z, Li F, Duan X. Study on the mechanism and kinetics of the thermal decomposition of Ni/Al layered double hydroxide nitrate. Ind Eng Chem Res. 2008;47:7211–8.
17. Ay AN, Zümreoglu-Karan B, Temel A, Mafra L. Layered double hydroxides with interlayer borate anions: a critical evaluation of synthesis methodology and pH-independent orientations in nanogalleries. Appl Clay Sci. Submitted for publication.
18. Coats AW, Redfern JP. Kinetic parameters from thermogravimetric data. Nature. 1964;201:68–9.
19. Sharp JH, Wentworth SA. Kinetic analysis of thermogravimetric data. Anal Chem. 1969;41:2060–2.
20. Kolcu O, Zümreoğlu-Karan B. Nonisothermal dehydration kinetics of sodium-light lanthanoid double sulfate monohydrates. Thermochim Acta. 1997;296:135–9.
21. Moura AO, Prado AGS. Effect of thermal dehydration and rehydration on Na-magadite structure. J Colloid Interface Sci. 2009;330:392–8.
22. Salentine CG. High-field boron-11 NMR of alkali borates. Aqueous polyborate equilibria. Inorg Chem. 1983;22:3920–4.
23. Simon JM, Smith RA. Borate raw materials. Glass Technol. 2000;41:169–73.
24. Weir MR, Kydd RA. Synthesis of metatungstate pillared layered double hydroxides with variable layer composition. Effect of the Mg:Al ratio on the microporous structure. Micropor Mesopor Mat. 1998;20:339–47.
25. Rives V. Characterization of layered double hydroxides and their decomposition products. Mater Chem Phys. 2002;75:19–25.
26. Palmer SJ, Spratt HJ, Frost RL. Thermal decomposition of hydrotalcites with variable cationic ratios. J Therm Anal Calorim. 2009;95:123–9.
27. Wegrzyn A, Rafalska-Lasocha A, Majda D, Dziembaj R, Papp H. The influence of mixed anionic composition of Mg-Al hydrotalcites on the thermal decomposition mechanism based on in situ study. J Therm Anal Calorim. 2010;99:443–57.